An experimental study of the potential for fault reactivation during changes in gas and pore-water pressure.

Robert J. Cuss and Jon F. Harrington, British Geological Survey, Keyworth, Nottingham, NG12 5GG, UK

Corresponding author: R.J. Cuss, British Geological Survey, Keyworth, Nottingham, NG12 5GG, UK (rjcu@bgs.ac.uk).

Abstract: *The injection of CO_2 into a depleted reservoir will alter the pore pressure, which if sufficiently perturbed could result in fault reactivation. This paper presents an experimental study of fault reactivation potential in fully saturated kaolinite and Ball Clay fault gouges. Clear differences were observed in fault reactivation pressure when water was injected, with the addition of mica/illite in Ball Clay seen to reduce the pressure necessary for reactivation. Slip occurred once pore-pressure within the gouge was sufficient to overcome the normal stress acting on the fault. During gas injection localised dilatant pathways are formed with approximately only 15 % of the fault observing an elevated gas pressure. This localisation is insufficient to overcome normal stress and so reactivation is not initiated. Therefore faults are more likely to conduct gas than to reactivate. The Mohr approach of assessing fault reactivity potential gave mixed results. Hydro-mechanical coupling, saturation state, mineralogical composition and time-dependent features of the clay require inclusion in this approach otherwise experiments that are predicted to be stable result in fault reactivation.*

Highlights

- The shear apparatus allowed fault reactivation to be observed and investigated for variations in clay gouge mineralogy

- Reactivation pressure related to yield strength and starting shear strength in kaolinite and Ball Clay respectively
- Gas not able to initiate fault reactivation with faults becoming conductive to gas as opposed to creating slip
- Mohr-circle approach to assessing safe pressure changes insufficient to predict reactivation

Keywords

Fault reactivation; multiphase flow; kaolinite; Ball Clay; shear testing.

1.0 Introduction

The capture of CO_2 from large point source emitters and storage in the form of a super-critical fluid within geological formations has been identified as a key technology in tackling anthropogenic climate change (Haszeldine, 2009; Bickle, 2009). To achieve a reduction in emissions, significant quantities of CO_2 need to be injected into suitable geological formations capable of containing the fluid for thousands of years. It has been estimated that approximately 30 billion barrels of CO_2 need to be injected annually (Zoback & Gorelick, 2012). Several demonstration projects have been conducted injecting megatonne scale CO_2 into depleted hydrocarbons reservoirs, such as at Sleipner (Norwegian North Sea; Arts *et al.*, 2008), Weyburn (Saskatchewan Province, Canada; Wilson *et al.*, 2004) and In Salah (Algeria; Mathieson *et al.*, 2010). Storage of CO_2 in depleted reservoirs offers the security of storage with an effective top-seal that previously acted as a seal to hydrocarbons.

The use of a depleted reservoir will play a role in the performance of the storage facility. During depletion, pore pressure within the reservoir will have been lowered during hydrocarbon extraction and as a result the reservoir will have subsided. The injection of super-critical fluid into a depleted reservoir will result in the opposite, with pore pressure increased and heave of the reservoir. The use of injection and extraction boreholes can minimise this effect, with water injected at a rate similar to the extraction rate of the hydrocarbon during drawdown, and extraction of aquifer water at a similar rate to CO_2 injection during carbon sequestration. Local deformation will still occur though if the two boreholes are well spaced, as seen during the In Salah CO_2 storage project in Algeria (Mathieson *et al.*, 2010). Perturbations of the reservoir pore fluid pressures are required in order to initiate flow out of, or into the reservoir. These changes in pore pressure, and as a result the stress state, may result in undesired geomechanical deformation that could affect the integrity of the overlying seal. Zoback & Gorelick (2012) identified the risk to security from a geomechanical point of view, while Economides & Ehlig-Economides (2009) showed that an upper pressure limit exists for CCS, above which the seal is potentially compromised due to the formation of fractures. However, Vilarrasa & Carrera (2015) state that large earthquakes are unlikely to be triggered during CO_2 injection in sedimentary basins and therefore leakage is not likely to be induced. Verdon *et al.* (2013) examined the deformation observed at injection sites and noted that the geomechanical response was complicated and non-intuitive at Weyburn, small at Sleipner due to the high permeability of the reservoir, and uplift and microseimic activity was noted at In Salah. Therefore, reservoirs need to be considered on an individual basis based on their geometry and the properties of the geology present.

Hydraulic and mechanical interactions play a critical role in reactivating faults at various scales in the Earth's upper crust (Scholz, 1990). Injection of fluid and the resulting changes in the stress-state can result in the reactivation of existing faults (Cappa & Rutqvist, 2011; Segall & Rice, 1995), which can result in felt seismicity. This has occurred in geothermal projects (e.g. Bachmann *et al.*, 2012; Gan & Elsworth, 2014), waste water injection during shale gas exploration (e.g. Ellsworth, 2013), during hydraulic fracturing (e.g. Clarke *et al.*, 2014; Holland, 2013), and by natural gas injection at the Castor storage site in Spain (Cesca *et al.*, 2014). However, only micro-seismicity has been observed during Carbon Capture and Storage (Verdon *et al.*, 2013).

Faults with high clay content within the fault core may have a permeability as low as 10^{-22} m^2 (Faulkner & Rutter, 2000). Such flow barriers within a reservoir may increase overpressure locally, which could result in fault reactivation (Rutqvist *et al.*, 2007; Rinaldi *et al.*, 2015). This may create an open migration pathway for CO_2 to escape from the reservoir (Zoback & Gorelick, 2012), although no correlation between seismicity and leakage was found in numerical modelling (Rinaldi *et al.*, 2014[a,b]). Experimental work related to fault reactivation has tended to look at mechanical controls using analogue sand-box experiments (Krantz, 1991; Richard & Krantz, 1991; Dubois *et al.*, 2002; Bellahsen & Daniela, 2005; Del Ventisette *et al.*, 2006) or examining the flow properties of fault gouge and inferring fault weakness on geomechanical response (Crawford *et al.*, 2008; Faulkner & Rutter, 2000; Faulkner & Rutter, 2001).

Modelling studies of fault reactivation potential, or slip tendency, have been conducted by several workers; some of which are summarised here, see Rutqvist (2012) for a more comprehensive summary of numerical modelling. Streit & Hillis (2004) estimated fault stability for underground storage of CO_2 based on the Mohr-Coulomb approach of predicting individual fault strength. A similar approach using slip tendency analysis using the 3-dimensional Mohr-space has been proposed by Leclère & Fabbri (2013). Williams *et al.* (2015) calculated slip tendency based on the ratio of shear to normal stress for faults within the Moray Firth, North Sea, to determine which were critically stressed. A critically stressed fault is one where the shear stresses acting upon the fault is at the limit of the frictional strength of the fault, i.e. as soon as stress is increased on the fault it will result in slip. They found that pore fluid increases as modest as several kPa were sufficient to cause reactivation for certain fault segments, with a maximum pore pressure of 20 MPa. However, Zhang *et al.* (2015) used a coupled geomechanical–fluid flow modelling approach and demonstrated that reactivation wasn't likely in the South West Hub of Western Australia. Coupled reservoir-geomechanical numerical modelling (Rutqvist, 2011) has been used to simulate fault/fracture zone reactivation induced by CO_2 injections (Cappa & Rutqvist, 2012; Rinaldi & Rutqvist, 2013) to assess the potential for fault instability and shear failure (Cappa & Rutqvist, 2011). Gan & Elsworth (2014) modelled the role of both pore fluid change and temperature drawdown on fault reactivation in relation to geothermal projects and showed that temperature variations needed to be considered when examining fault stability.

A fault will remain locked as long as the applied shear stress is less than the strength of the contact. Karl Terzaghi first showed in 1923 that pore-fluid under pressure has a profound effect on the physical properties of porous solids (Terzaghi, 1943). In a saturated porous system, the fluid supports some proportion of the applied load lowering the overall stress exerted through grains. Strength is therefore determined not by confining pressure alone, but by the difference between confining and pore-pressures. Hubbert & Rubey (1959) showed this applies to faults; a pore pressure of P_f reduces the frictional strength of faults (τ), which can be represented by a criterion of Coulomb form:

$$\tau_f = C + \mu\sigma_n' = C + \mu(\sigma_n - P_f) \quad [1]$$

where C is the cohesive strength of the fault, μ is the coefficient of friction, σ_n, is the normal stress on the fault, and $'$ denotes effective stress. Byerlee (1978) showed that μ ranges between 0.6 and 1.0, but can be approximated as 0.75 ± 0.15 (Sibson, 1994). Fault reactivation can therefore occur when shear stress along the fault (τ) equals τ_f. This condition can occur through an increase in shear stress, decrease in normal stress, or an increase in fluid pressure.

This paper presents results from an experimental study aimed at evaluating fault reactivation potential within the laboratory in two fault gouges. The current study represents the second stage of a three-part investigation of the potential for fault reactivation during the sequestration of carbon dioxide. The three parts of the study were; 1) the role of stress history on fault flow properties, as reported in Cuss *et al.* (2016); 2) quantification of fault reactivation potential as a result of elevated pore pressure (the current study); and 3) the role of stress history on fault reactivation. The scenario being investigated is for a static boundary condition for stress acting on a fault with an increase in pore pressure initiating fault reactivation; therefore directly simulating an increase in pore pressure in response to the injection of CO_2 during sequestration. The objectives of the study were:

- Investigate whether fault reactivation could be detected using a shear apparatus with an angled fault-plane within the laboratory;
- Investigate the mechanical properties of two clay gouges during shear;
- Variation in fault reactivation behaviour between two clay gouges;
- Variation in fault reactivation potential as a result in elevation of gas or water pressure.

In order to simulate a critically stressed fault, gouge material was sheared to a stress representative of the residual shear strength before pore pressure was elevated. This ensured that the fault plane was actively stressed. Equation (1) shows that the coefficient of friction dictates the strength of a fault, although cohesion also contributes to fault strength. Two clay gouges were selected so as to determine whether different material properties would alter the potential for fault reactivation, or whether a single parameter could be used to estimate the stress state at failure for different gouge compositions. The primary aim of the study was to establish maximum pore pressure perturbations that could be employed during carbon sequestration.

Previous experimental work at the British Geological Survey (BGS) on fracture transmissivity in Opalinus clay (Cuss *et al.*, 2011; 2014[a,b]) and kaolinite gouge (Sathar *et al.*, 2012) showed that hydraulic flow is a complex, focused, transient property that is dependent upon stress history, normal stress, shear displacement, fracture topology, fluid composition, and clay swelling characteristics. The current experimental program aimed to extend this knowledge by investigating the potential for fault reactivation by elevating pore pressure within gouge filled discontinuities.

2 Experimental setup

All experiments were performed using the bespoke Angled Shear Rig (ASR, Figure 1) designed and built at the BGS. Previous experiments conducted on Opalinus Clay (Cuss *et al.*, 2009; 2011; 2014[b]) showed that fracture topology is a key parameter in controlling fluid flow along fractures. In order to reduce the number of variables required to fully understand flow, an analogue discontinuity with smooth fracture surfaces was investigated. The surfaces of the discontinuity were machined from steel and therefore flow could only occur through the fault gouge within the discontinuity.

The ASR (Figure 1) comprised of 5 key components:

1. Rigid body that had been designed to have a bulk modulus of compressibility and shear modulus approximately 2 orders of magnitude greater than the clay gouge tested, resulting in minimal deformation of the apparatus compared to the test sample;
2. Vertical load system comprising an Enerpac hydraulic ram that was controlled using a Teledyne/ISCO 260D syringe pump, a rigid loading frame and an upper thrust block (up

to 20 MPa vertical stress, 72 kN force). The Enerpac ram had a stroke of 105 mm, which meant that it could easily accommodate the vertical displacement of the top block as it rode up the fault surface at constant vertical load. Note: The vertical stress created by the ram is not equal to the normal stress perpendicular to the fault plane and represents the maximum principal (vertical) stress within a reservoir;

3. Shear force actuator comprised of a modified and horizontally mounted Teledyne/ISCO 500D syringe pump designed to drive shear as slow as 14 microns a day at a constant rate (equivalent to 1 mm in 69 days) along a low friction bearing;
4. Pore pressure system comprising a Teledyne/ISCO 500D syringe pump that could deliver either water or gas up to a pressure of 25.8 MPa. The syringe pump delivered fluid through the centre of the top block directly to the fault surface.
5. A state-of-the-art custom designed data acquisition system using National Instruments LabVIEW™ software facilitating the remote monitoring and control of all experimental parameters.

The experimental fault assembly consisted of precision machined 316 stainless steel top and bottom blocks (thrust blocks) with a dip of 30 degrees with respect to horizontal (the shearing direction). The thrust blocks were polished so as not to introduce preferential pathways for flow. The top block was connected to the vertical loading arrangement by means of a swivel mechanism which was engaged to the shoulders on either side of the top block. Care was taken in the design of the swivel mechanism so as to negate rotation and tilting of the top blocks and shear mechanism. Two pore pressure transducers, attached to ports which were positioned orthogonally to each other at 15 mm from the central pore fluid inlet allowed measurement of pore pressures within the fault gouge (see Figure 1). The thrust blocks of the apparatus were made with a contact area of 60 mm × 60 mm. The lower thrust block was longer than the top one so that the contact area of the experimental discontinuity could be maintained constant throughout the test.

As shown in Figure 1, the shear force actuator acted upon the angled bottom-block of the apparatus. The movement of the bottom-block was measured using a linear variable differential transducer (LVDT), which had a full range of ± 25 mm and an accuracy of 0.5 µm. Vertical travel of the thrust block was measured by a high precision non-contact capacitance displacement transducer, which had a full range of ± 0.5 mm and an accuracy of 0.06 µm. Horizontal load was measured using a load cell fitted laterally to the top-block. This measured the force resultant from lateral movement of the bottom block transmitted through the clay gouge.

Gouge material for the experiments was prepared from either powdered kaolinite or Ball Clay (as described in Table 1); 16 ± 0.1 g of de-ionized water was added to 20 ± 0.1 g of oven dried clay powder. The water and clay were then stirred for five minutes giving a fully saturated paste. The mixed paste was smeared uniformly onto the surface of the top block, which was then carefully lowered onto the bottom block thus forming a paste gouge. The initial thickness of the gouge was in the order of 1 mm. However, as no lateral confinement was made of the clay gouge, thickness decreased to approximately 70 ± 10 µm with loading up to 10 MPa and clay was squeezed from between the thrust blocks; this excess material acted as a buffer preventing water from the shear bath entering the fault gouge or causing sloughing. No lateral gouge confinement was included as this would require sealing elements that would have a high frictional component along the fault surface compared with the low frictional properties of the clay.

Twenty-eight experiments are described in this paper (Table 2); of these, 13 were fault reactivation experiments conducted using water as the injected fluid, 7 were fault reactivation experiments conducted with gas as the injection fluid, and the remaining 8 are reported only for mechanical data. For all 28 experiments the first stage was to conduct a shear experiment. Once the apparatus had been assembled, vertical stress was increased in steps up to the desired magnitude. Vertical stress was kept constant by the Teledyne/ISCO syringe pump for the remainder of the experiment. The shear actuator was initiated to give 1 mm of strain over a 24 hour period; this equated to a strain-rate of 1.93×10^{-7} s^{-1}. Data were logged every minute throughout the experiment. Within the 24-hour long shear experiment, the gouge had achieved stable peak stress sliding. After approximately 24 hours the shear actuator was turned off and constant pressure was maintained in the vertical loading ram.

Fault reactivation experiments were performed by injecting fluid into the central port of the top thrust block. For water injection, de-ionised water was injected at a constant pressure of 0.25 MPa throughout the shear experiment. Once stable pressure had been achieved, the injection syringe pump was switched to a constant flow-rate of 0.25 ml h^{-1}, sufficient to raise pore fluid pressure within the fault gouge to 10 MPa over a 24-hour period. For gas injection experiments, an interface vessel was filled with 170 ml of helium at a pressure of 2 MPa. Cuss *et al.* (2015) showed that the gas entry pressure of kaolinite gouge was in excess of 5 MPa, therefore a starting pressure of 2 MPa would not result in gas flow within the gouge. The injection syringe pump was switched to constant flow rate operation and delivered 10 ml h^{-1} of water into the base of the interface vessel, raising the pressure within the gas to sufficient levels to allow gas entry within a 5 hour time-frame. Helium was selected as the permeant as it is inert and to allow direct comparison with previous experiments (Sathar *et al.*, 2012; Cuss *et al.*, 2015). Fault reactivation was observed as an instantaneous reduction in shear stress and change in vertical displacement of the load frame. Some tests showed single movements, others showed multiple slip events, whilst some tests showed no sign of reactivation.

Once the time of fault reactivation was known, it was possible to determine the vertical and horizontal stress at reactivation. Pore pressure was calculated as the average pore pressure within the fault gouge, this being more representative of the force acting to oppose normal stress over the complete fracture surface as opposed to the maximum pore pressure, which represented a localised increase. As shown in Figure 1, radial flow was assumed from the central injection filter. This would result in a pore pressure gradient as shown in Figure 8a, giving an average pore pressure within the gouge of 0.35 P_p, where P_p is the injection pressure. The recorded vertical and horizontal stress components were rotated to represent normal and shear stress. Throughout this paper, vertical and horizontal stresses are referred to when discussing far-field stresses, whereas normal and shear stress are used to discuss the local stress on the fault.

Gas entry-pressure was determined using the methodology described in Cuss *et al.* (2015), by comparing the pressure predicted from Boyle's law with the observed gas pressure. Using the ideal gas law it is possible to determine the mass flux into the clay gouge. A departure is seen between predicted and observed once gas starts to enter the clay; from this the gas entry pressure is then derived.

3 Experimental results

A total of 28 tests were conducted during the current study, as shown in Figure 2 and Table 2; of these, 22 were conducted on kaolinite and 6 were Ball Clay. All 28 tests are reported here for their mechanical shear content, the initial stage of each test was identical for all tests. Following shearing, a total of 20 of the tests were conducted as fault reactivation experiments; a total of 13 water-injection reactivation experiments were conducted, 7 gas-injection.

Figure 2 shows the results for the 24-hour long shear tests conducted, with all tests conducted with the same protocols irrespective of whether they were fault reactivation tests or not, or whether they were gas or water injection. Tests on kaolinite gouge ranged in vertical stress from 1.1 to 6.4 MPa, while for Ball Clay the range was 2.6 to 6.3 MPa. As shown in Figure 2a and b, good repeatability was seen during repeat testing at given vertical stresses for both kaolinite and Ball Clay gouges. Figure 2c shows an example result for test ASR_BigCCS_11K and the four parameters that can be calculated for each test. The starting shear stress is simply the magnitude of stress observed before shear was initiated. The initial stress-strain response was linear, the slope of which described the shear modulus. In most tests, this was observed as a well-defined linear response, the deviation from which describes the yield shear stress. The yield stress was determined as the departure from the linear region by 0.02 MPa; all tests were checked that this criterion was appropriate and that a similar result was being achieved as would be by manual identification. The final shear stress parameter identified was peak shear stress. As shown in Figure 2, all tests showed classic elasto-plastic behaviour. Therefore the peak stress condition also describes the residual strength of the gouge. Table 2 outlines the vertical and shear stress for the start, yield, and peak shear stress conditions.

Figure 3 and Table 3 show the results for starting, yield, and peak shear stresses for all experiments in the current study. As can be seen, the data describe linear relationships with few outliers. Linear regression is shown in Figure 3 with the intercept set to zero; as shown in Table 3, this does not significantly reduce the R^2 achieved showing that it is a good approximation. Comparing the trends for kaolinite and Ball Clay shows that Ball Clay has a higher starting shear stress; therefore the starting condition is not simply the translation of vertical stress into the horizontal direction with the difference being due to the mineralogical difference of the two clays. Ball Clay, however, has lower yield strength with a much reduced linear relationship observed between stress and strain. Ball Clay is also a weaker material and is not able to sustain as high a shear stress as kaolinite. Therefore the addition of illite, quartz, and possibly water content are resulting in a reduced strength compared with pure kaolinite. Figure 4 shows the data for shear modulus; as shown in Table 2 tests ASR_BigCCS_19BC and ASR_BigCCS_25Kg gave anomalously low and high shear moduli respectively. Figure 4 shows that kaolinite is a more stiff material when stress is below 5.5 MPa, with Ball Clay showing greater stiffness above this condition. However, considerable spread is seen in the kaolinite data compared to Ball Clay, with R^2 of 0.37 and 0.95 respectively. The slope of peak shear stress represents the coefficient of friction (μ), whilst the intercept represents the cohesion (C) of the material, as shown in Figure 4b. From this parameter it is possible to derive the angle of internal friction (ϕ) and fault angle (θ), as shown in Table 4, from the relationships:

$$\mu = tan\phi \qquad \text{and} \qquad \phi = 90° - 2\theta \qquad [2]$$

Figure 5a-c shows an example result from fault reactivation test ASR_BigCCS_14BC using water as the injection fluid. As shown (Figure 5a), the injection of fluid at a constant rate increased the pore fluid pressure in the fault from the starting average pore pressure of 0.1 MPa up to 9 MPa over a 24-hour period. As pore pressure rose, a series of slip events were initiated, as shown by a reduction in shear stress (Figure 5b) and change in vertical displacement (Figure 5c). A total of nine slips occurred, with the first occurring at an average pore pressure in the gouge of 1.27 MPa. The time between slip events decreased with subsequent slip events, this was not related to the increase in pore pressure gradient with time as the pore pressure between slip events also decreased. Therefore the gouge was undergoing strain softening as a result of reactivation, with further slip events taking less energy to initiate.

All 13 reactivation tests conducted resulted in slip of the critically stressed fault plane as a result of elevated pore pressure, results are shown in Figure 6, Table 2, and Table 3. The reactivation pressure is defined as the pore pressure that is sufficient to initiate fault reactivation and slip. Kaolinite gouge showed good repeatability for the three tests conducted at 2.7 MPa vertical stress. A linear relationship is seen between reactivation pressure and vertical stress, with a value of R^2 of 0.91 (Figure 6a, Table 3). This is reduced to 0.39 when the intercept is set to zero, with this suggesting that reactivation in kaolinite gouge is controlled by the yield strength of the clay. A less well defined linear relationship is observed for Ball Clay, with a value of R^2 of 0.56 (Figure 6b, Table 3); note that tying the intercept to zero does not significantly alter the statistics. The results suggest that the initial starting stress controls the reactivation pressure. This indicates that Ball Clay has little strength and that the first slip occurs once vertical stress has been overcome. Plotting reactivation pressure against vertical stress (Figure 6c) shows that both clays form similar relationships with differences in the intercept, which may be related to the difference in relative strength of the two clays. However, plotting the data in the differential stress versus effective mean stress space (Figure 6d) gives a single fault reactivation envelope for both clays.

During gas injection, the addition of water in the base of the interface vessel results in an exponential increase in gas pressure dependent on the starting volume of the gas and the change in volume, which is related to the rate at which the syringe pump delivers water into the vessel. The form of the pressure response can be predicted from Boyle’s law, as can the STP (standard temperature pressure) flow of gas into the fault gouge. Initially the STP flow rate is very small and rises gradually but then the rate of increase of the flow rate abruptly increases. The pressure at which this occurs is identified as the gas entry pressure. Gas peak pressure is simply the maximum gas pressure experienced. Gas breakthrough is the pressure when gas was able to reach the outside of the top block, resulting in a reduction in gas pressure. Table 5 shows the gas entry and maximum gas pressure for all gas injection experiments. Note that test ASR_BigCCS_22Kg was started from 2.5 MPa, which was greater than the gas entry pressure.

The results for the fault reactivation tests conducted on kaolinite using gas as the injection fluid markedly contrast with the results seen for water injection (Figure 5d-f, Table 2). Only one test resulting in evidence of fault reactivation, as shown in Figure 5d-f. Assuming radial flow, this occurred at an average pore pressure within the gouge of 1.65 MPa, which is lower than that seen during water injection (average of 2.1 MPa). As shown in Figure 5d, fault reactivation resulted in increased flow into the gouge, as seen by a marked change in slope of pore pressure, this increased until gas pressure peaked at 5.58 MPa, when gas injection was stopped. This was followed by a reduction in pressure to approximately 1 MPa as gas escaped along a conductive pathway between the injection filter and the outside of the gouge. The reduction of gas pressure accelerated at Day 1.13, suggesting that a further gas pathway had managed to reach breakthrough.

Figure 7 shows the results from the fault reactivation experiments using gas as the permeant. No sensitivity to vertical stress was observed in gas entry pressure or the maximum gas pressure achieved (Figure 7a). Only one experiment resulted in fault reactivation. As seen, gas pressure was not able to achieve the level observed during water injection, except for one test conducted at a low vertical stress of 1.13 MPa. However, this test did not show any signs of fault reactivation. Figure 7b shows that no significant differences were apparent in shear stress between tests conducted with gas or water injection. As plotted, the shear stress at gas entry and that during reactivation with water entry perfectly correspond, clearly demonstrating that mechanically there were no differences between the two types of test.

4 Discussion

The current study successfully reproduced fault reactivation in the laboratory and allowed differences to be noted between water and gas injection, as well as variations related to clay gouge mineralogy.

The mechanical aspects of the current study produced well constrained data for two fault gouges. Very good repeatability was seen for repeat tests conducted at near identical boundary conditions. Well constrained linear relationships were noted for starting, yield and peak shear stress. Few outliers were seen in all tests and these occurred in the starting shear stress. These tend to remain unexplained and are probably due to small shear movements occurring during the setup of the experiment. It should be noted that the anomalous data points did not result in anomalous yield or peak strength results; strengthening the assumed hypothesis of shear movement during setup. As starting shear stress is not the primary dataset these are not viewed as problematic. The differences between the starting shear stress for the two gouges is likely to represent variations in cohesion. Although zero cohesion has been assumed, a better fit to the Ball Clay data is achieved with cohesion of 0.33 MPa (Table 4), whereas little change is seen in kaolinite. However, the addition of quartz and mica/illite results in more vertical stress being translated into the horizontal direction, suggesting that Ball Clay is a weaker material with less frictional strength. This is also apparent in the peak stress condition and lower coefficient of friction. This observation is in contrast with Crawford *et al.* (2008), who showed that sheared gouge samples showed a continuous reduction in frictional strength with increasing clay fraction. This suggests that either the mica/illite content played a significant role in weakening the gouge, or that the nature (grain size, roundness etc) differed between the two studies. It could also be a result in variations in clay saturation, although in all tests the gouge was close to 100 % saturation. Figure 4 shows that the results from this study correspond with Byerlee's law (Byerlee, 1978) and therefore that the measured values are consistent with natural rocks.

The fault reactivation study was able to clearly identify reactivation. However, some hydraulic injection tests resulted in single reactivation, whereas others resulted in multiple slip-events (see Figure 5b). The cause for this is uncertain. One hypothesis may be that a larger single slip event releases more energy than a smaller one. However, no variation in shear stress reduction or magnitude in dilation was observed. In general, all slip events using water tended to have similar magnitudes in shear stress reduction and dilation. Variations in the number of slip events were seen for the four tests conducted with a kaolinite gouge at a vertical stress of about 2.6 MPa. Figure 8a shows the assumed pore pressure distribution within the fault gouge. Cuss *et al.* (2011) reported that not all of a fracture surface in Opalinus Clay was conductive during hydraulic flow and that deformation along a sheared fracture was localised into zones of differing texture. It is possible that the initial pore pressure distribution is similar to that described by Figure 8a, but as slip occurs the gouge is modified resulting in parts becoming conductive, whilst other parts are self-sealed by the shear movement. In tests that showed limited slip events it is possible that the gouge contained conductive channels following shear that resulted in pore pressure dissipation and pressure not increasing as expected. In tests that did show multiple slip-events, these channels did not result in pore pressure dissipation and pressure continued to ramp, becoming sufficient to cause further slip events. Data is not available to fully determine the reasons for these observations.

The results for hydraulic injection produced reliable data that showed a marked difference between the two clay gouges. As shown in Figure 6, reactivation tended to occur when the average pore pressure exceeded the yield strength of kaolinite, whereas in Ball Clay reactivation occurred at a stress below the initial starting shear strength. This results in two different reactivation envelopes as shown in Figure 6c. This clearly shows that mica/illite and/or quartz reduces the stress at which a fault will reactivate. However, considering data in the effective mean stress versus differential stress space (*Q*-*P*) results in a well constrained single reactivation envelope, as seen in Figure 6d. Effective mean stress (*P*) is defined simply as the mean stress minus the effect of pore pressure, i.e. $P = ((\sigma_1 + \sigma_2 + \sigma_3)/3) - P_f$. The differential stress (*Q*) is simply defined as the difference between the maximum and minimum principal stresses, i.e. $Q = \sigma_1 - \sigma_3$. This suggests that in *Q*-*P*, mineralogy plays no role in determining reactivation. This envelope suggests that reactivation will occur when differential stress is 2.5 times the effective mean stress:

$$Q = 2.5P \qquad [3]$$

This relationship can be used to determine the pore pressure likely to cause fault reactivation along existing features. Therefore the likelihood of fault reactivation is dependent on pressure within the storage reservoir, the magnitude of which will depend on the quantity of fluid injected and the flow properties of the reservoir.

A marked difference was noted for fault reactivation when gas was injected into the clay gouge. In general, it can be stated that fault reactivation was not possible when gas was injected. As shown in Figure 8a, modelled pore pressure distribution in the clay gouge assuming radial flow would result in a pore pressure of approximately 300 kPa at the monitoring pore pressure filter location on the fault surface given the experimental boundary conditions. However, Figure 8b shows typical data recorded during gas and water injection experiments (tests reported in Cuss *et al.*, 2014[a]), showing that pore pressure within the gouge was significantly less than 300 kPa. For the case of gas injection the pore pressure observed in the gouge was effectively atmospheric, indicating no elevation of pore pressure as a result of gas injection. All tests were typical of this response. In order to understand gas and water flow in clay gouge a number of observations can be drawn upon. In Cuss *et al.*, (2011) it was reported that less than 50 % of a fracture surface was hydraulically conductive in Opalinus Clay, as identified from the injection of fluorescein. In Sathar *et al.* (2012) it was reported that localised streams of bubbles were seen following gas breakthrough in injection experiments. These observations led to the development of the Fracture Visualisation Rig (see Wiseall *et al.*, 2015). Using a 50 mm thick 110 mm diameter quartz fused glass window, water and gas injection into clay gouge can be observed. As shown in Figure 8c, the injection of gas into a kaolinite gouge results in the formation of a number of dilatant gas pathways, until a pathway reaches the outside of the apparatus and facilitates breakthrough, resulting in the elastic closure of the dilatant pathways. This helps to explain the low pore pressure within the gouge, with no pathway intercepting the pore pressure observation ports. As reported in Cuss *et al.* (2012[a]; 2014[a]), clay rich materials are able to sustain very high pressure gradients when gas is injected. Even when gas is flowing, the elevated gas pressure is not transmitted to the bulk pore fluid. Therefore this is not a phenomena restricted to the geometry of the current experimental apparatus, the clay gouge selected, or saturation of the gouge.

Figure 9 shows the conceptual model to explain the differences seen between water and gas injection. During water injection, radial flow is observed resulting in a pore pressure distribution within the clay gouge. The force exerted perpendicular to the fault can be equated as the average pore pressure within the gouge. This means that an elevated pressure sufficient to overcome cohesion within the gouge is possible, resulting in slip. In the case of gas injection, localised dilatant gas pathways are formed. This compresses the clay walls either side of the pathway, but results in only a localised perturbation of the clay. Although large gas pressures may be present within the dilatant features, the average pore pressure within the gouge is much less than for corresponding pressures of water injection. Figure 8d suggests that a maximum of 15 % of the gouge would be made of dilatant gas pathways, meaning that the force exerted perpendicular to the fault would be much less than for water injection; a multiplier of injection pressure of 0.35 for water and 0.14 for gas. The flow properties of kaolinite and Ball Clay are such that it is much easier for a dilatant pathway to form and propagate to a condition of breakthrough, than it is to result in an average force sufficient to overcome the vertical stress and cohesion of the gouge, which would result in slip.

One anomalous observation was the single gas injection experiment that resulted in fault reactivation (test ASR_BigCCS_23Kg). This occurred at a gas pressure of 4.71 MPa, which is less than the absolute water pressure (average of 6 MPa) seen to cause reactivation during hydraulic testing. As discussed above, pore pressure is not well transmitted from the gas phase to the water-saturated clay, as seen by low pore pressure within the gouge. Therefore, the upward force acting on the surfaces of the fault would be highly localised. Each test was conducted as identical as practicable, using the same mixture of clay, setting up procedures, quantity of gas, and gas injection rate. As seen in Figure 2a and Table 2, the mechanical part of the experiment gave near identical results for test ASR_BigCCS_23Kg as ASR_BigCCS_26Kg, the latter of which did not reactivate. However, Figure 5 clearly shows a reactivation event at a time that does not correspond with initial gas entry, with a small reduction in shear stress and change in vertical displacement. This shear movement resulted in an increased gas flow into the gouge. Repeating the experiment (test ASR_BigCCS_26Kg) and conducting a further experiment at lower vertical stress (test ASR_BigCCS_27Kg) showed no evidence of reactivation. Close examination of the test data for test ASR_BigCCS_23Kg has not identified anything different between this and the non-reactivating gas injection tests and the reason for slip remains undetermined.

Gas transport properties showed no sensitivity to vertical stress, with a constant gas entry and maximum gas pressure. Part one of the current study, as defined in the introduction and reported in Cuss *et al.* (2016), examined the hydraulic flow properties of kaolinite gouge as a function of vertical stress. This data showed a clear reduction in hydraulic transmissivity of kaolinite gouge, reducing from 4.3 to 1.5 × 10^{-14} m^2 s^{-1} between a vertical stress of 0.8 and 10

MPa. Such a reduction would be expected for gas flow. As described in Cuss *et al.* (2015), repeat testing in the current apparatus resulted in a repeatable gas entry pressure, but once gas flow was initiated, little repeatability in flow properties was observed. This was attributed to differences in the number and distribution of pathways, as shown during fracture visualisation tests (Wiseall *et al.*, 2015; Figure 8c). The pressure at which gas pathways form is reproducible as dictated by the strength of the gouge. Once formation begins, the number of pathways arbitrarily alters and therefore transport properties also vary. It would be expected that as the gouge is compressed to a greater degree by increased vertical stress that gas entry would increase. However, the nano-metre scale of clay minerals means that the entry pressure is not altered. This might change at greater vertical stresses or if gouge was not able to be squeezed out from between the thrust blocks. Cuss *et al.* (2015) report the variation in flow properties for fractures of varying orientation to the shear direction under constant vertical stress. Experiments conducted at 0, 15, 30 and 45° degrees to the shear orientation at constant vertical stress can be viewed as variations in normal stress to a single fracture. As with the current study, little variation in gas entry pressure was observed.

The primary aim of this study was to test experimentally the controls on fault reactivation and the safe operational pressure limits of CCS. It is common to apply Mohr-Coulomb concepts to estimate fault reactivation potential and therefore the current study is presented in Mohr space in Figure 10, . with the frictional sliding envelope determined from the coefficient of friction shown in Figure 4b. The fault angle represents the slip-plane with respect to the direction of shear. For the current experimental set-up the 2-D Mohr circle has been used, with the size of the Mohr circle bound by the vertical stress and the horizontal stress.

Some tests resulted in fault reactivation at a pressure very close to that predicted by the Mohr approach (e.g. Figure 10a,b). Contrary, tests shown in Figure 10c,d show that reactivation occurred at a stress far below the pressure predicted from the frictional sliding envelope.

These tests show a stress state that should be stable. Figure 10e shows an example of a test where reactivation occurred at a pore pressure greater than predicted. Generally these results are mixed. Some tests are successfully predicted, some under-estimated and some over-estimated. An under-estimate of pore-pressure variation is acceptable, where an over-estimate means that faults that are predicted to be stable would in fact slip. Figure 10f shows the results for the single gas test that resulted in reactivation. As seen, the Mohr approach shows that reactivation should have occurred at this gas pressure and that the approach would appear valid. However, Figure 10g,h show that at least three tests, with possibly a fourth, were at a stress condition where reactivation should have been observed. Therefore the localised nature of gas pathway formation is not fully accounted for in the approach. Given the mixed results, caution needs to be used when using the Mohr approach to determining fault reactivation potential. Should a maximum pore pressure be restricted to 0.5 – 0.75 of the pore pressure predicted by the Mohr approach then this approach may be satisfactory.

The Mohr-Coulomb approach to predicting fault reactivation is used by many studies reported, e.g. Cappa & Rutqvist, 2011, 2012; Rinaldi & Rutqvist, 2013; Rinaldi et al., 2015. The current study suggests that as a first approximation the approach is valid, although the complete prediction of the pore-pressure is more complex. This may be due to artefacts of the experimental set-up or be associated with complex coupling that occurs as a result of the hydro-mechanical properties of the clay gouge that are not fully described by the simplified approach presented here. It is clear that this is an area that requires further research in order to fully appreciate the physics driving fault reactivation. The observations of the current study also suggest that free-gas will not result in fault reactivation. However, it should be acknowledged that the experimental geometry meant that gas was able to drain from the fault gouge and that in nature sufficient quantities of gas may become present within faults to initiate reactivation.

One limitation of the current study was not being able to inject super-critical CO_2. Therefore the emphasis of the study was on changes in pore-water pressure as a result of CO_2 injection and should free-gas be present in the reservoir, the consequence of elevated gas pressure on existing faults. The influence of super-critical CO_2 directly in contact with faults was not investigated, nor was the influence of CO_2 should a gaseous phase form. The study was conducted at low pressures compared with in situ stress states and further investigation is needed to determine whether similar findings would be found at representative reservoir pressures.

5 Conclusions

This paper presents results from an experimental study of 28 shear tests on a simulated fault angled 30° to the shear direction with a fault gouge of kaolinite or Ball Clay. The main conclusions of the study were:

- Mechanical data showed good repeatability, with Ball Clay having less frictional strength, but becomes stiffer than kaolinite at vertical stresses greater than 5 MPa. Good linear relationships were seen for starting, yield and peak shear stress; the latter corresponding to the coefficient of friction for the gouge material, with achieved results correspond with Byerlee's law.
- The addition of mica/illite and/or quartz reduces the cohesive strength of the gouge. As Crawford *et al.* (2008) showed that quartz content increases the frictional properties it is likely that mica/illite is responsible for the reduction in cohesion.
- Fault reactivation occurred at pressure related to the yield strength in kaolinite and at a pressure less than the starting shear stress in Ball Clay. This shows that Ball Clay has a much lower frictional strength than kaolinite. A single envelope was achieved for fault reactivation potential when data were viewed in the differential (Q) versus effective

mean stress (P) space; stating reactivation will occur when $Q = 2.5\ P$. This suggests that the Q-P representation is irrespective of mineralogy, at least for the range of conditions tested in the current work.

- During gas injection, only one test showed reactivation and this occurred at a pressure predicted by the Mohr approach. However, 3 further tests predicted to slip showed no evidence of movement.
- Gas entry and maximum gas pressure showed no pressure sensitivity to vertical stress. The gas entry pressure is dictated by the frictional properties of the clay gouge, which do not significantly alter over the range of vertical stresses investigated. The maximum pressure achieved is also related to the frictional properties and therefore also showed little to no sensitivity to vertical stress over the limited stresses investigated.
- Gas injection results in localised discrete pathways, with pressure elevated in approximately 15 % of the fault area. This means that the average pressure exerted normally to the fault is not sufficient to induce slip. During hydraulic injection the pore pressure distribution is more evenly dispersed and results in a greater normal force that is sufficient to initiate slip. No difference is seen in the mechanical data, demonstrating that the lack of reactivation is only due to the localisation of gas flow.
- The frictional properties of the fault gouge dictate that it is more likely to become conductive to gas than to reactivate.
- The Mohr approach of assessing fault reactivity had mixed results, but is generally viewed as a valid approach. Some tests had good predictions of pore pressure at reactivation, whilst most where either under or over-estimated. An over-estimate of pore pressure adds a safety margin to predictions and is acceptable. However, an under-estimate in gas pressure means that faults predicted to be stable may in reality reactivate. Given the mixed results, caution needs to be used when using the Mohr approach to

determining fault reactivation potential. A safety margin can be used to ensure that favourably oriented faults do not reactivate. In the simple form presented, the Mohr-Coulomb approach did not capture the full complexity observed. This is likely a result of flow localisation resulting in complex pore-pressure distributions or due to hydro-mechanical coupling, which is complex in clays.

Acknowledgements

The study was undertaken by staff of the Minerals and Waste Program of the BGS using the experimental facilities of the Transport Properties Research Laboratory (TPRL). The authors would like to thank the skilled staff of the Research & Development Workshops at the BGS, in particular Humphrey Wallis, for their design and construction of the experimental apparatus. This publication has been produced with support from the BIGCCS Centre. The BIGCCS Centre is part of the Norwegian research programme Centres for Environment-friendly Energy Research (FME) and is funded by the following partners: ConocoPhillips, Gassco, Shell, Statoil, TOTAL, Engie and the Research Council of Norway (193816/S60). The BGS authors publish with the permission of the Executive Director, British Geological Survey (NERC).

References

Arts, R.J., Chadwick, R.A., Eiken, O., Thibeau, S., and Nooner, S. (2008) Ten years' experience of monitoring CO_2 injection in the Utsira Sand at Sleipner, offshore Norway. *First Break*, **26**, pp.65–72.

Bachmann, C.E., Wiemer, S., Goertz-Allmann, B.P., and Woessner, J. (2012) Influence of pore-pressure on the event-size distribution of induced earthquakes. *Geophysical Research Letters*, **39** (9): L09302.

Bellahsen, N., and Daniel, J.M. (2005). Fault reactivation control on normal fault growth: an experimental study. *Journal of Structural Geology*, **27**(4), pp.769-780.

Bickle M.J. (2009) Geological carbon storage. *Nature Geoscience*, **2**, pp.815–818.

Byerlee, J.D. (1978) Friction of rocks. *Pure Applied Geophysics*, **116**, pp.615–626.

Cappa, F., and Rutqvist, J. (2011) Modeling of coupled deformation and permeability evolution during fault reactivation induced by deep underground injection of CO_2. *International Journal of Greenhouse Gas Control*, **5**(2), pp.336-346.

Cappa, F., and J. Rutqvist (2012) Seismic rupture and ground accelerations induced by CO_2 injection in the shallow crust. *Geophysical Journal International*, **190**(3), pp.1784–1789.

Cesca, S., Grigoli, F., Heimann, S., Gonzalez, A., Buforn, E., Maghsoudi, S., Blanch, E., and Dahm, T. (2014) The 2013 September–October seismic sequence offshore Spain: a case of seismicity triggered by gas injection? *Geophysical Journal International*, **198**, pp.941–953.

Clarke, H., Eisner, L., Styles, P., and Turner, P. (2014) Felt seismicity associated with shale gas hydraulic fracturing: The first documented example in Europe. *Geophysical Research Letters*, **41**(23), pp.8308-8314.

Crawford, B.R., Faulkner, D.R., and Rutter, E.H. (2008) Strength, porosity, and permeability development during hydrostatic and shear loading of synthetic quartz-clay fault gouge. *Journal of Geophysical Research*, **113**, B03207, doi:10.1029/2006JB004634.

Cuss, R.J., Graham, C.C., Wiseall, A.C, and Harrington, J.F. (2016) Cyclic loading of an idealized clay-filled fault; comparing hydraulic flow in two clay gouges. Geofluids. In press.

Cuss, R.J., Harrington, J.F., Graham, C.C., and Noy, D.J. (2014[a]) Observations of Pore Pressure in Clay-rich Materials; Implications for the Concept of Effective Stress Applied to Unconventional Hydrocarbons. European Geosciences Union General Assembly 2014, EGU Division Energy, Resources & the Environment (ERE). *Energy Procedia*, **59**, pp.59-66; doi:10.1016/j.egypro.2014.10.349

Cuss, R.J., Harrington, J.F., Graham, C.J., Sathar, S., and Milodowski, T. (2012[a]) Observations of heterogeneous pore pressure distributions in clay-rich materials. *Mineralogical Magazine*, December 2012, Vol. **76**(8), pp.3115-3129. DOI: 10.1180/minmag.2012.076.8.26

Cuss, R.J., Harrington, J.F., Milodowski, A.E., and Wiseall, A.C. (2014[b]) Experimental study of gas flow along an induced fracture in Opalinus Clay. *British Geological Survey Commissioned Report*, **CR/14/051**. 79pp.

Cuss, R.J., Harrington, J.F., Sathar, S., and Norris, S. (2015) An experimental study of the flow of gas along faults of varying orientation to the stress-field; Implications for performance assessment of radioactive waste disposal. *Journal of Geophysical Research – Solid Earth*. **120**, pp.3932-3945, doi:10.1002/2014JB011333

Cuss, R.J., Milodowski, A., and Harrington, J.F. (2011) Fracture transmissivity as a function of normal and shear stress: first results in Opalinus clay. *Physics and Chemistry of the Earth*. **36**, pp.1960-1971. DOI: 10.1016/j.pce.2011.07.080

Cuss, R.J., Milodowski, A.E., Harrington, J.F. and Noy, D.J. (2009) Fracture transmissivity test of an idealised fracture in Opalinus Clay. *British Geological Survey Commissioned Report*, **CR/09/163**. 74pp.

Del Ventisette, C., Montanari, D., Sani, F., & Bonini, M. (2006) Basin inversion and fault reactivation in laboratory experiments. *Journal of Structural Geology*, **28**(11), 2067-2083.

Donohew, A.T., Horseman, S.T., and Harrington, J.F. (2000) Gas entry into unconfined clay pastes at water contents between the liquid and plastic limits. In: Environmental Mineralogy: Microbial Interactions, Anthropogenic Influences, Contaminated Land and Waste Management; Cotter-Howells, J.D., Campbell, L.S., Valsami-Jones, E., and Batchelder, M. (eds). *Mineralogical Society Series*, **9**. Mineralogical Society, London. Pp. 369-394 ISBN 0 903056 20 8.

Dubois, A., Odonne, F., Massonnat, G., Lebourg, T., and Fabre, R. (2002) Analogue modelling of fault reactivation: tectonic inversion and oblique remobilisation of grabens. *Journal of Structural Geology*, 24(11), 1741-1752.

Economides, M.J., and Ehlig-Economides, C.A. (2009) Sequestering Carbon Dioxide in a Closed Underground Volume. *Society of Petroleum Engineers*, Richardson, TX, SPE 124430.

Ellsworth, W.L. (2013) Injection-induced earthquakes. *Science*, **341**: 6142.

Faulkner, D.R., and Rutter, E.H. (2000) Comparisons of water and argon permeability in natural clay-bearing fault gouges under high pressure at 20 C. *Journal of Geophysical Research*, **105**, pp.16,415–16,426.

Faulkner, D.R., and Rutter, E.H. (2001) Can the maintenance of overpressured fluids in large strike-slip fault zones explain their apparent weakness? *Geology*, **29**, pp.503–506.

Gan, Q., and Elsworth, D. (2014) Analysis of fluid injection-induced fault reactivation and seismic slip in geothermal reservoirs. *Journal of Geophysical Research*, Solid Earth, **119**, pp.3340–3353, doi:10.1002/2013JB010679.

Haszeldine, R.S. (2009) Carbon capture and storage: How green can black be? *Science*, **325**(5948): pp.1647–1652.

Highley, D.E. (1984) China Clay. Mineral Dossier No. 26. Mineral Resources Consultative Committee, HMSO, London.

Holland, A. (2013) Earthquakes triggered by hydraulic fracturing in south-central Oklahoma, *Bull. Seismol. Soc. Am.*, **103**, pp.1784–1792.

Hubbert, M.K. and Rubey, W.W. (1959) Role of fluid pressure in the mechanics of overthrust faulting. *Bull. geol. Soc. Am.*, **70**, pp.115-205

Krantz, R.W. (1991) Measurements of friction coefficients and cohesion for faulting and fault reactivation in laboratory models using sand and sand mixtures. *Tectonophysics*, **188**(1-2), pp.203-207.

Leclère, H., and Fabbri, O. (2013) A new three-dimensional method of fault reactivation analysis. *Journal of Structural Geology*, **48**, pp.153-161.

Mathieson, A., Midgley, J., Dodds, K., Wright, I., Ringrose, P., and Saoul, N. (2010) CO_2 sequestration monitoring and verification technologies applied at Krechba, Algeria. *The Leading Edge*, **29**(2), pp.216-222.

Pereira, L.C., Guimarães, L.J., Horowitz, B., and Sánchez, M. (2014) Coupled hydro-mechanical fault reactivation analysis incorporating evidence theory for uncertainty quantification. *Computers and Geotechnics*, **56**, pp.202-215.

Richard, P., and Krantz, R. W. (1991) Experiments on fault reactivation in strike-slip mode. *Tectonophysics*, **188**(1), pp.117-131.

Rinaldi, A.P., and Rutqvist, J. (2013) Modeling of deep fracture zone opening and transient ground surface uplift at KB-502 CO_2 injection well, In Salah, Algeria. *International Journal of Greenhouse Gas Control*, **12**, pp.155-167.

Rinaldi, A.P., Rutqvist, J., and Cappa, F. (2014a) Geomechanical effects on CO2 leakage through fault zones during large-scale underground injection. *Int. J. Greenh. Gas Contr.*, **20**, 171-131. doi:10.1016/j.ijggc.2013.11.001

Rinaldi, A.P., Jeanne, P., Rutqvist, J., Cappa, F., and Guglielmi, Y. (2014b) Effects of fault-zone architecture on earthquake magnitude and gas leakage related to CO_2 injection in a multi-layered sedimentary system. *Greenh. Gas Sci. Techn.*, **4**, 99-120. doi: 10.1002/ghg.1403

Rinaldi, A.P., Vilarrasa, V., Rutqvist, J., and Cappa, F. (2015) Fault reactivation during CO_2 sequestration: Effects of well orientation on seismicity and leakage. *Greenhouse Gases: Science and Technology*, **5**(5), pp.645-656.

Rutqvist, J., Birkholzer, J.T., Cappa, F. and Tsang, C.-F. (2007) Estimating maximum sustainable injection pressure during geological sequestration of CO_2 using coupled fluid flow and geomechanical fault-slip analysis. *Energ Conver Manage*, **48**, pp.1798–1807.

Rutqvist, J. (2011) Status of the TOUGH-FLAC simulator and recent applications related to coupled fluid flow and crustal deformations. *Computers & Geosciences*, **37**(6), pp.739-750.

Rutqvist J. (2012) The Geomechanics of CO2 Storage in Deep Sedimentary Formations. *Geotechnical and Geological Engineering*, **30**(3), 525-551.

Sathar, S., Reeves, H.J., Cuss, R.J., and Harrington, H.J. (2012) The role of stress history on the flow of fluids through fractures. *Mineralogical Magazine*. December 2012, Vol. **76**(8), pp.3165-3177. DOI: 10.1180/minmag.2012.076.8.30

Scholz, C.H. (1990) *The Mechanics of Earthquakes and Faulting*. Cambridge University Press, Cambridge, New York, Port Chester, Melbourne, Sydney.

Segall, P., and Rice, J.R. (1995) Dilatancy, compaction, and slip instability of a fluid-infiltrated fault, *Journal of Geophysical Research*, **100**(B11), pp.22,155–22,171, doi:10.1029/95JB02403.

Sibson, R.H. (1994) Crustal stress, faulting and fluid flow. *Geological Society, London, Special Publications*, **78**(1), pp.69-84.

Streit, J.E., and Hillis, R.R. (2004) Estimating fault stability and sustainable fluid pressures for underground storage of CO_2 in porous rock. *Energy*, **29**(9), pp.1445-1456.

Terzaghi, K. (1943) *Theoretical Soil Mechanics*. New York, John Wiley.

Verdon, J.P., Kendall, J.M., Stork, A.L., Chadwick, R.A., White, D.J., and Bissell, R.C. (2013) Comparison of geomechanical deformation induced by megatonne-scale CO_2 storage at Sleipner, Weyburn, and In Salah. *Proceedings of the National Academy of Sciences*, **110**(30), E2762-E2771.

Vilarrasa, V., and Carrera, J. (2015) Geologic Carbon Storage Is Unlikely to Trigger Large Earthquakes and Reactivate Faults through Which CO_2 Could Leak. *P. Natl. Acad. Sci. USA*, **112**(19), 5938-5943.

Williams, J.D.O. (2015) Analysis of in situ stress and fault reactivation potential for a major candidate storage aquifer. [Lecture] In: Trondheim Conference on CO_2 Capture, Transport and Storage, TCCS-8, Trondheim, Norway, 16-18 June 2015, Trondheim, Norway, 16-18 June 2015. (Unpublished)

Wilson, M., and Monea, M. (2004) IEA GHG Weyburn CO_2 monitoring & storage project. Summary report 2000-2004. Petroleum Technology Research Centre, Regina, SK, Canada.

Wiseall, A.C., Cuss, R.J., Graham, C.C., and Harrington, J.F. (2015) The visualization of flow paths in experimental studies of clay-rich materials. *Mineralogical Magazine*, **79**(6), pp.1335-1342.

Zhang, Y., Langhi, L., Schaubs, P.M., Delle Piane, C., Dewhurst, D.N., Stalker, L., and Michael, K. (2015) Geomechanical stability of CO_2 containment at the South West Hub Western Australia: A coupled geomechanical–fluid flow modelling approach. *International Journal of Greenhouse Gas Control*, **37**, pp.12-23.

Zoback, M.D., and Gorelick, S.M. (2012) Earthquake triggering and large-scale geologic storage of carbon dioxide. *Proc Natl Acad Sci* USA **109**(26), pp.10164–10168.

749

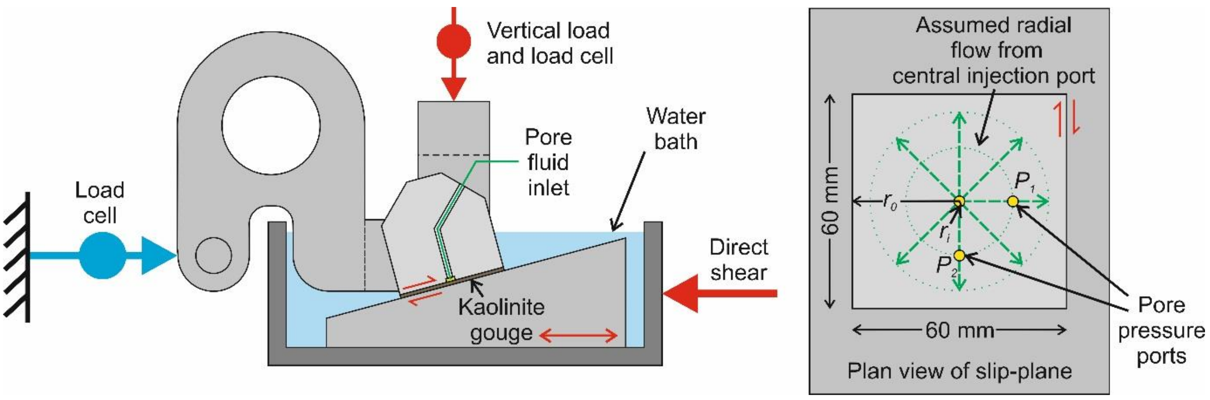

750 **Figure 1** Schematic of the Angled Shear Rig (ASR).

a)

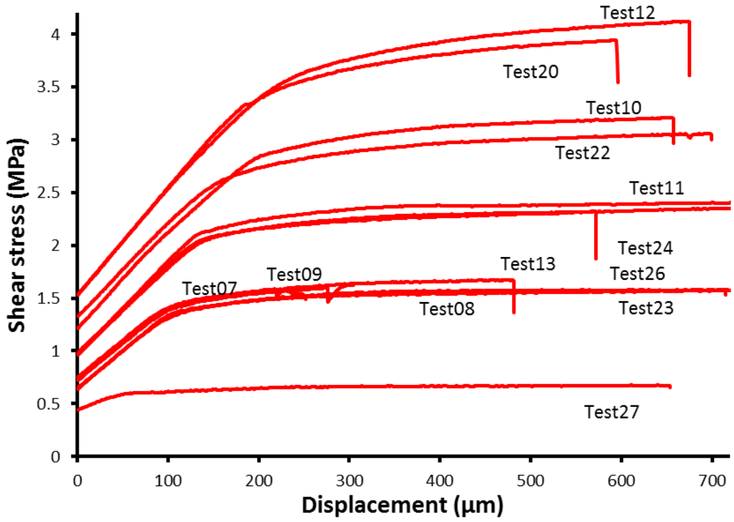
Shear stress (MPa)
Displacement (µm)
Test12
Test20
Test10
Test22
Test11
Test24
Test26
Test13
Test09
Test07
Test08
Test23
Test27
0
0.5
1
1.5
2
2.5
3
3.5
4
0
100
200
300
400
500
600
700

b)

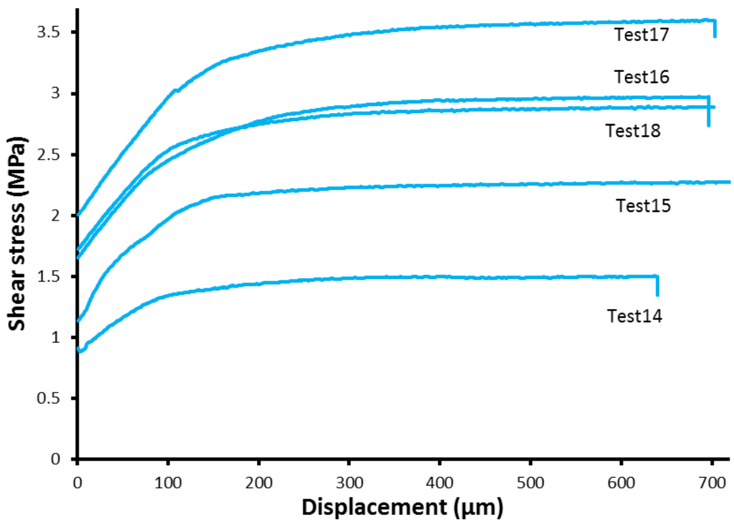
Shear stress (MPa)
Displacement (µm)
Test17
Test16
Test18
Test15
Test14
0
0.5
1
1.5
2
2.5
3
3.5
0
100
200
300
400
500
600
700

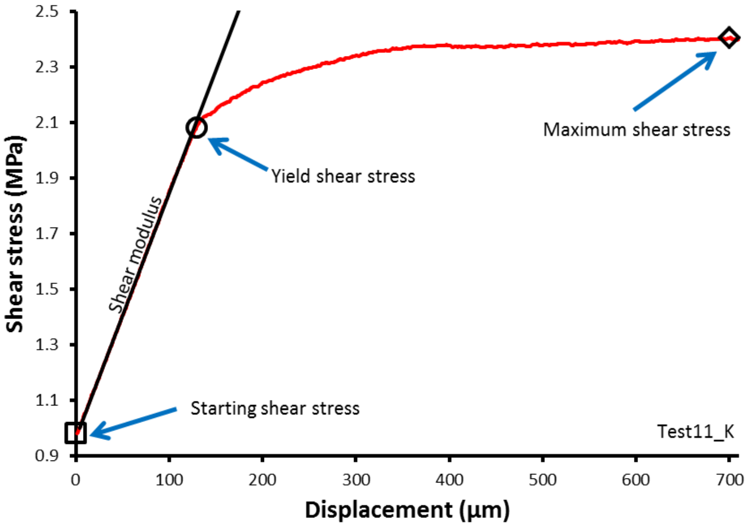
Shear stress (MPa)
Displacement (µm)
Shear modulus
Yield shear stress
Maximum shear stress
Starting shear stress
Test11_K
0.9
1.1
1.3
1.5
1.7
1.9
2.1
2.3
2.5
0
100
200
300
400
500
600
700

c)

Figure 2 Mechanical strength data for shear tests conducted on (a) kaolinite and (b) Ball Clay gouge materials. From these data it is possible to identify starting shear stress, yield shear stress, peak shear stress, and shear modulus (c).

a)

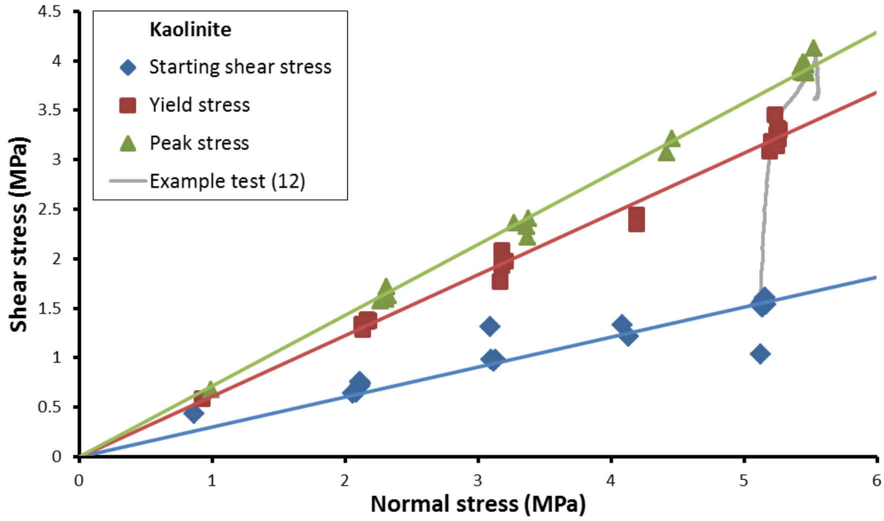

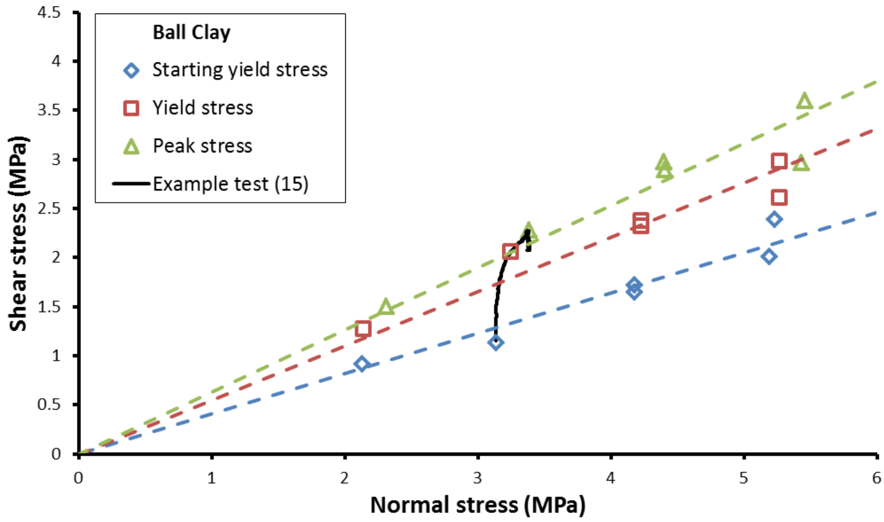

b)

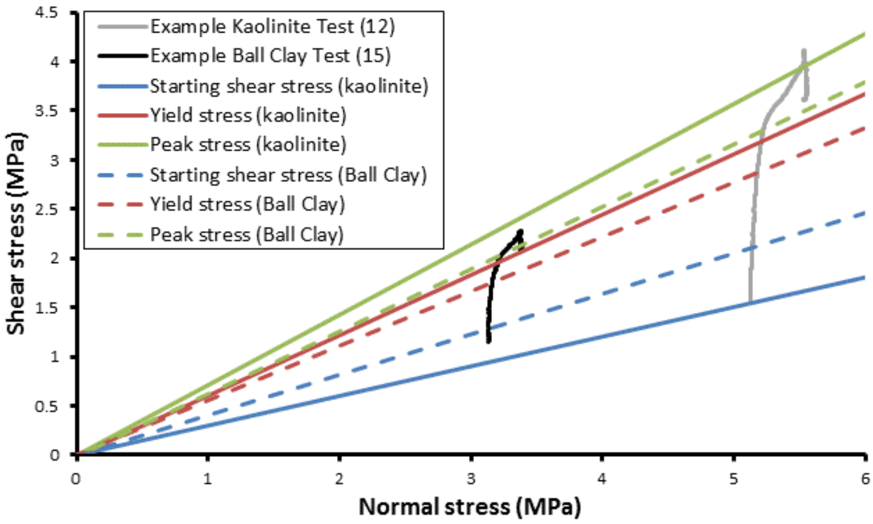

c)

Figure 3 Strength parameters for shear tests conducted on (a) kaolinite and (b) Ball Clay gouge materials. Clear linear trends are seen for the starting shear stress, the yield shear stress, and the peak shear stress. Comparison can be made between kaolinite and Ball Clay gouges (c).

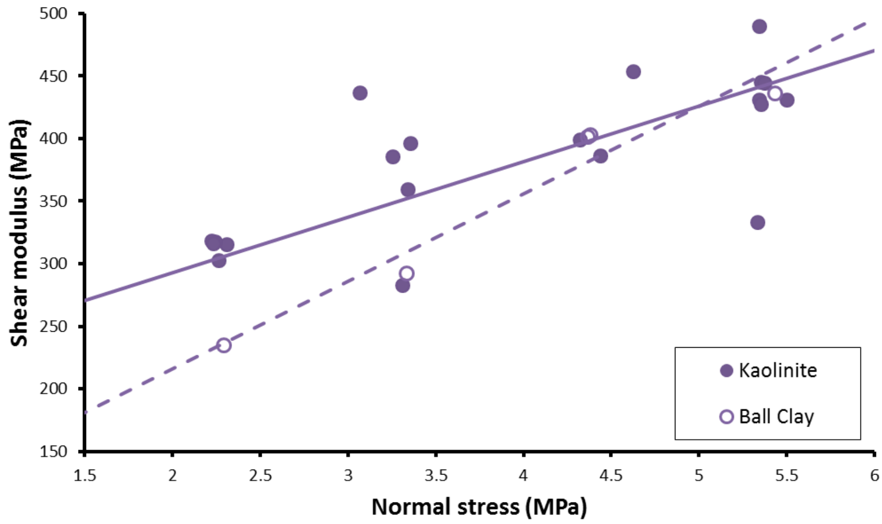

a

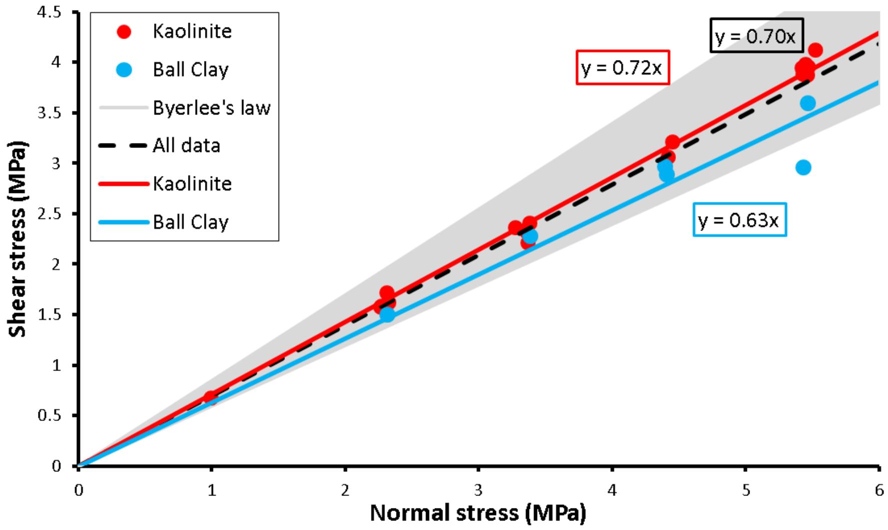

b

Figure 4 Shear properties for tests conducted on kaolinite and Ball Clay gouge. A) Shear modulus data. At stresses below 5 MPa it can be seen that kaolinite is a more stiff material, whereas Ball Clay becomes stiffer above these stress levels. B) Calculation of coefficient of internal friction, showing that the current data correspond to Byerlee's law (Byerlee, 1978).

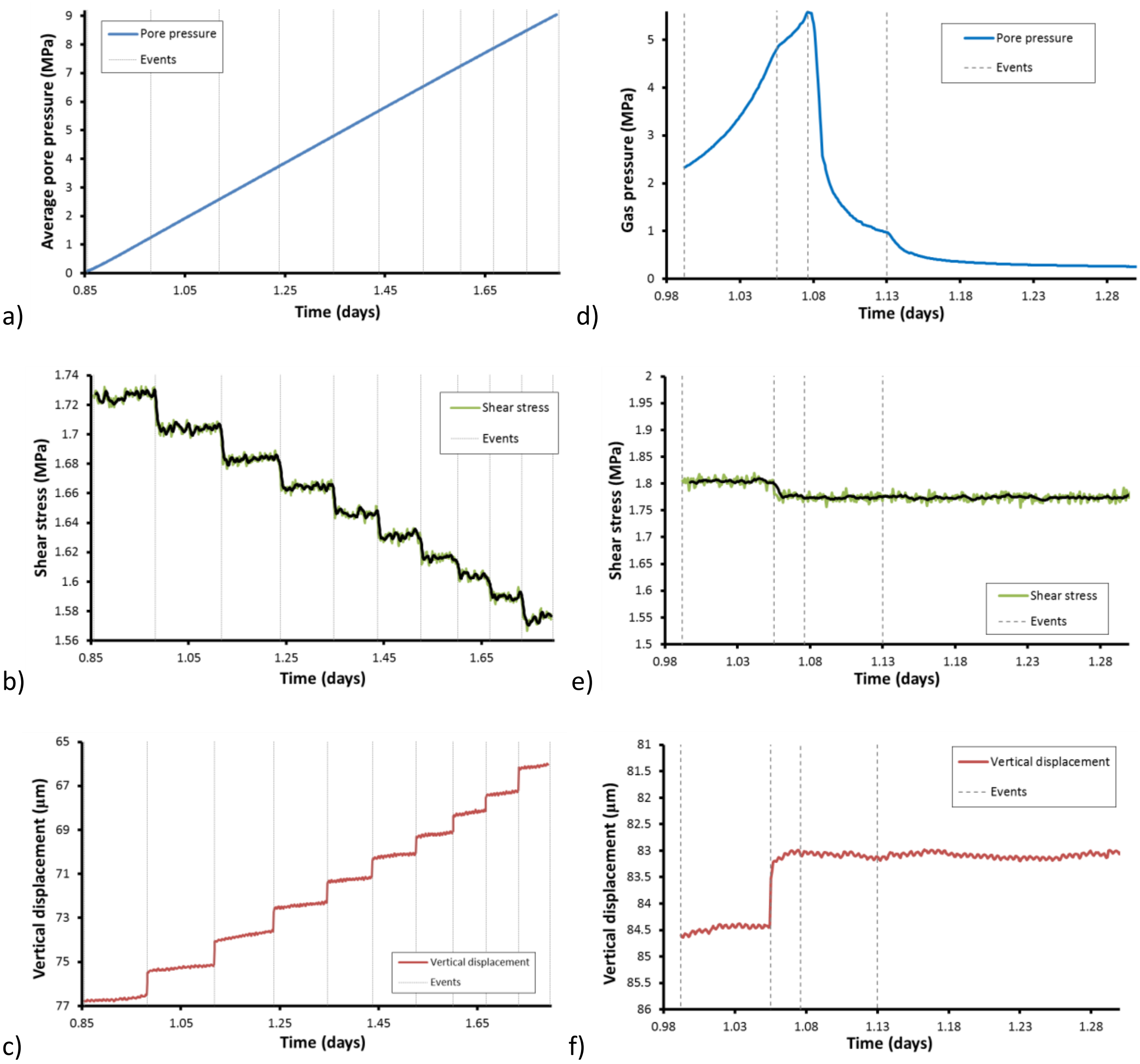

Figure 5 Example results from fault reactivation tests using water (a-c) and gas (d-f) as injection fluid. A) The injection of water creates a pore pressure increase. Fault reactivation is identified by a reduction in shear stress (b) and dilation on the fault plane (c). A total of 24 slip events were identified until the fault could no longer hold pore pressure. d) The injection of gas creates a pore pressure increase. Fault reactivation is identified by a reduction in shear stress (e) and dilation on the fault plane (f). As shown, only one slip event was identified. Gas flow is seen to increase following slip, as seen by a reduction in gas gradient (d).

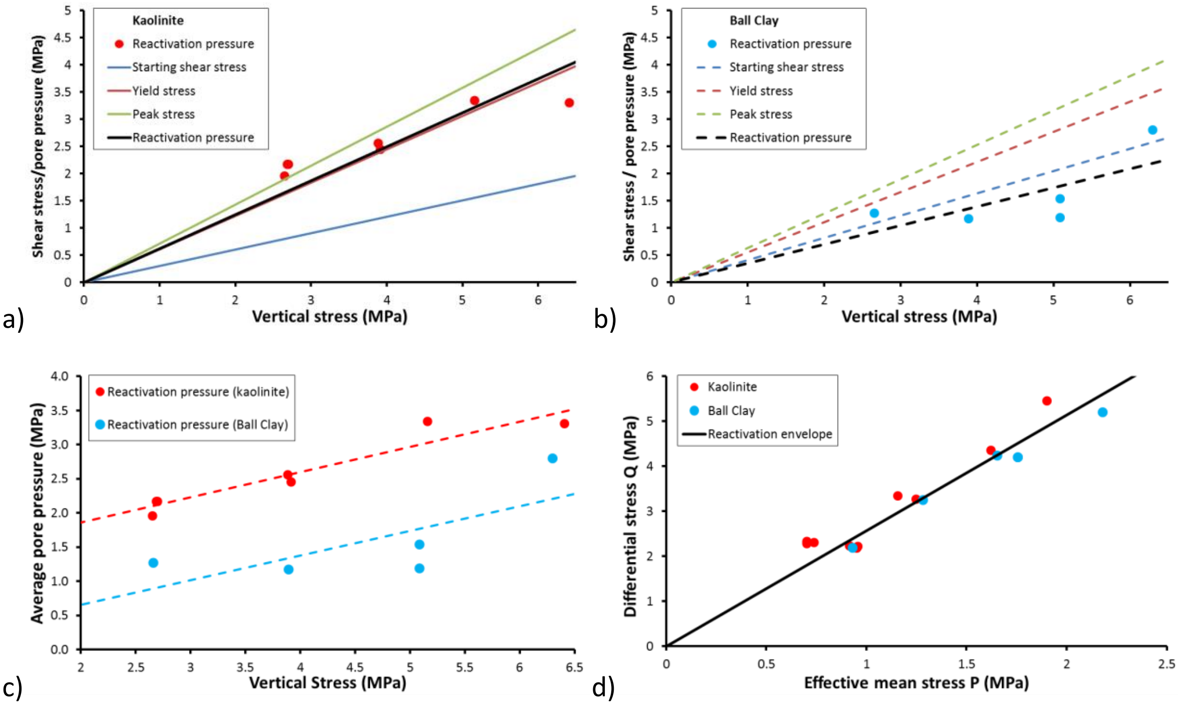

Figure 6 Results from the fault reactivation study using water as an injection fluid. A) Reactivation pressure for kaolinite can be seen to approximate the yield shear stress. B) In Ball Clay the reactivation stress approximates the starting shear stress. C) Plotting reactivation stress against vertical stress gives two relationships, whereas plotting data in the effective mean stress versus differential stress (Q-P) space gives a unified envelope for predicting fault reactivation (d).

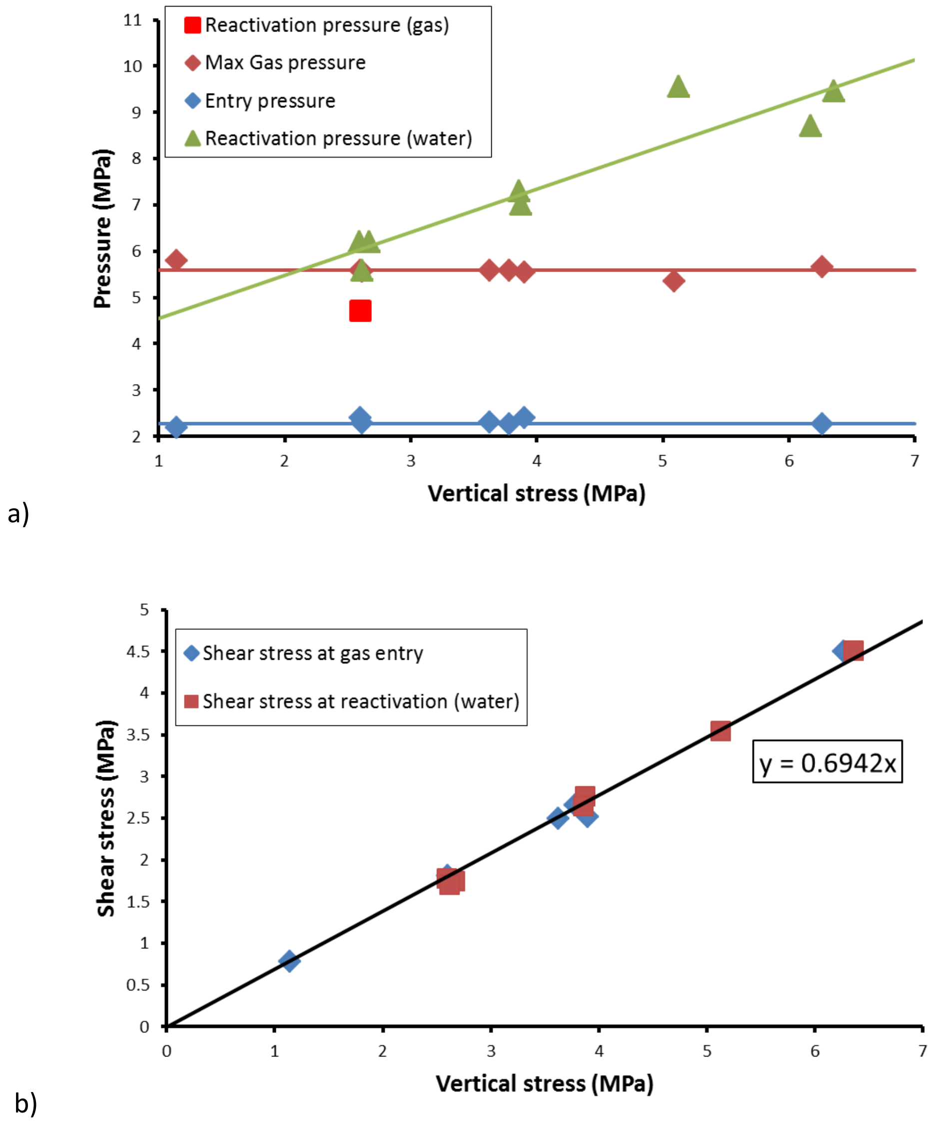

Figure 7 Results for fault reactivation using gas. A) Gas entry pressure and maximum gas pressure show no sensitivity to vertical stress loading. B) Comparing the shear stress at gas entry with the level seen at reactivation for water experiments shows no difference between the injection fluids.

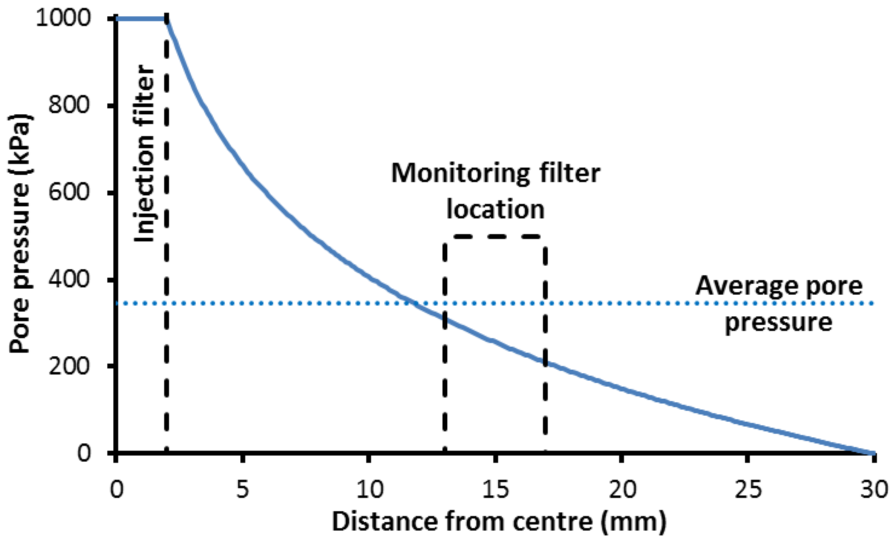

a)

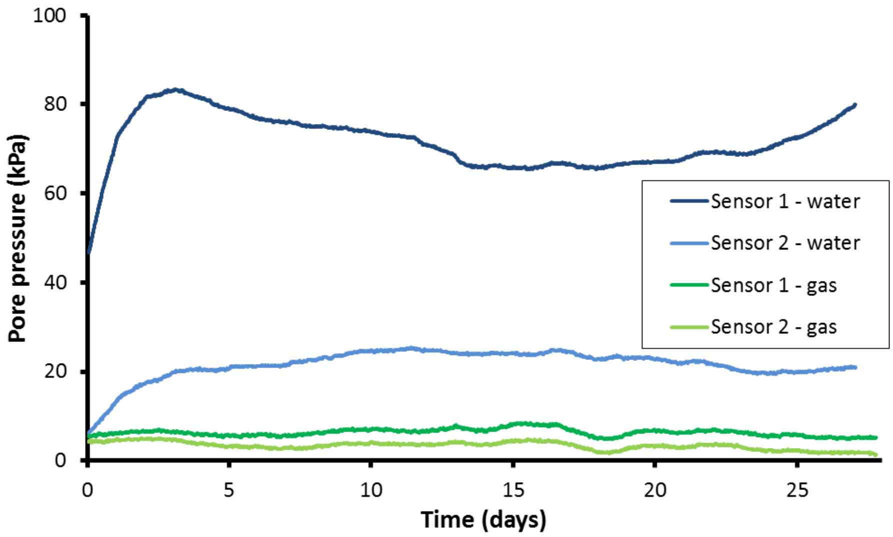

b)

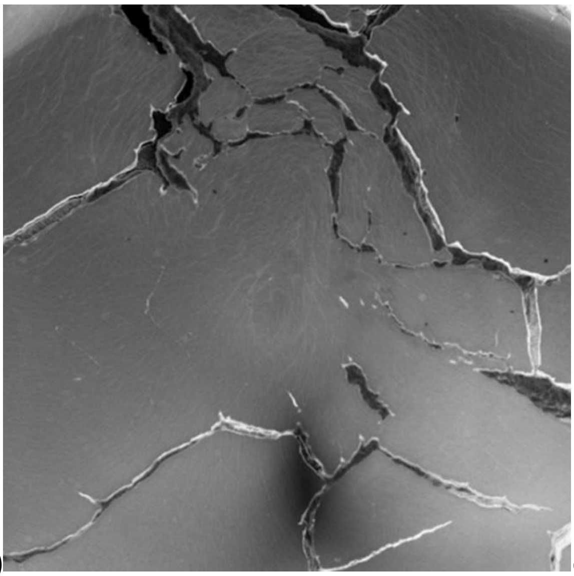

c)

d)

Figure 8 Observations of pore pressure within the fault gouge. A) Modelled result for pore pressure distribution assuming radial flow, indicating that pore pressure at the monitoring ports should be approximately 300 kPa. B) Observed pore pressure at the monitoring filter location shown in (a) during testing shows pore pressure is greatly below that modelled, with a very low pressure seen during gas injection (Cuss *et al.*, 2014[a]). C) Processed photograph from a Fracture Visualisation test showing a 60 × 60 mm square area with dilatant gas pathways. D) Location of pathways predicting < 15 % coverage.

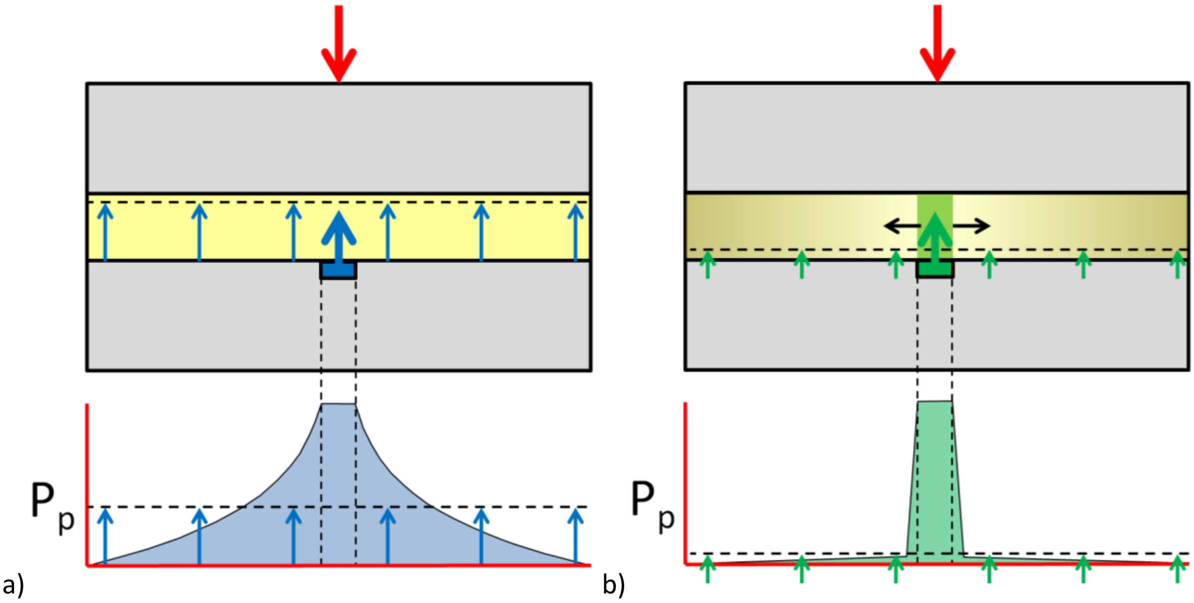

Figure 9 Model for fault reactivation. A) Water injection: The elevated water pressure results in a pore pressure profile as shown. The average pore pressure acting vertically is sufficient to cause fault reactivation. B) Gas injection: Pore pressure within the gouge is only locally increased by gas injection. The gouge compresses to accommodate dilatant pathways, as opposed to classical two-phase flow, resulting in a low average pore pressure acting vertically that isn’t sufficient to cause reactivation.

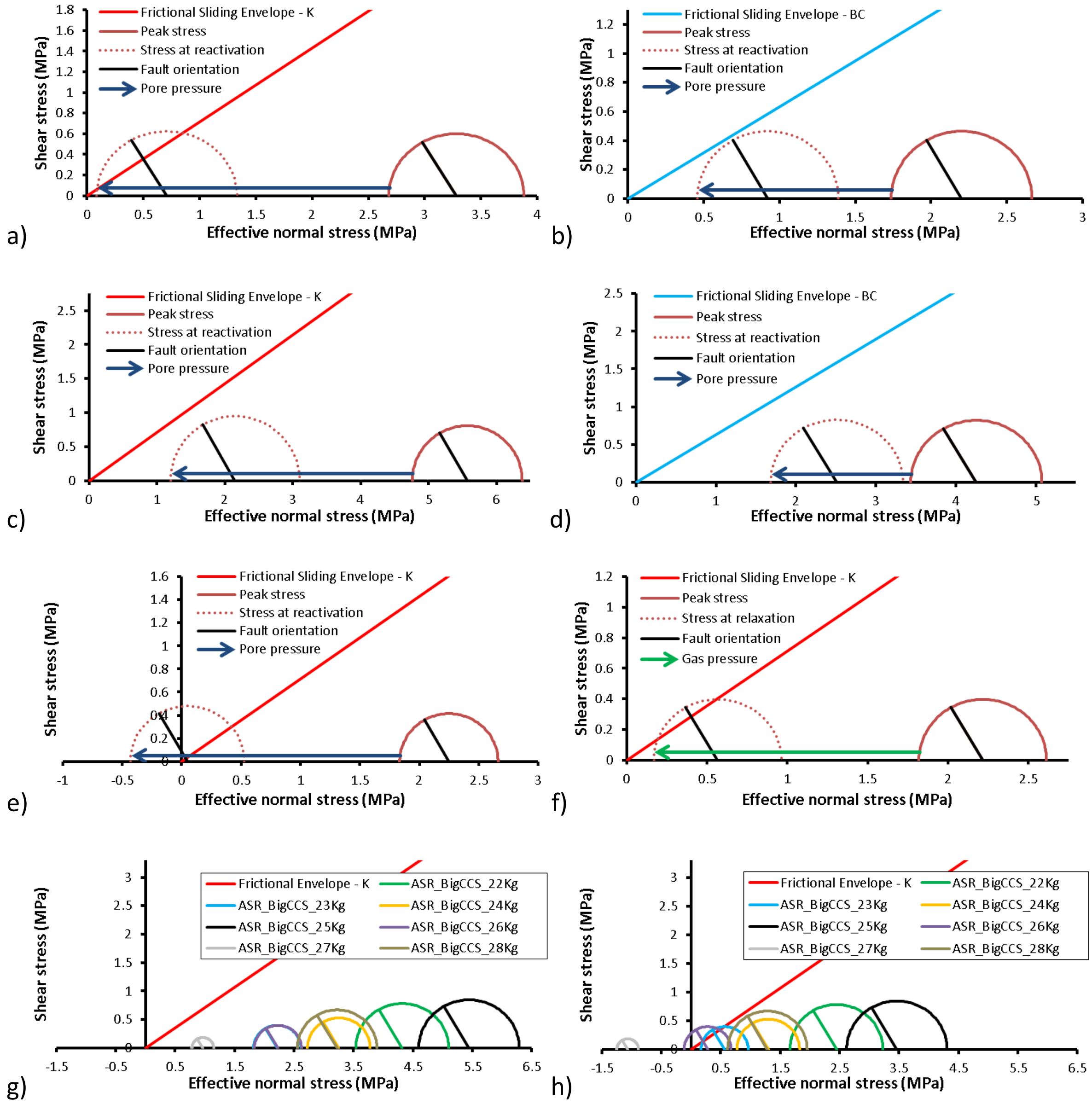

Figure 10 Representation of the test data in Mohr space. (a-b) Examples of where the Mohr approach gives good approximation for fault reactivation; (c-d) examples where reactivation occurred at pressures lower than the Mohr approach would predict; (e) example where reactivation didn't occur until a magnitude greater than predicted; (f) gas pressure sufficient to result in reactivation; (g-h) demonstration that four tests during gas injection would have been predicted to reactivate.

Gouge	Supplier	Geological information	Location	Composition
Kaolinite	Imerys	well-ordered form, coarse hexagonal platelets[1]	St Austell, UK	100 % kaolinite
Ball Clay		A1 seam; Tertiary, Poole Formation, Oakdale Clay Member)	Arne Clay Pit, Wareham, UK	37% kaolinite, 35% mica/illite and 26% quartz, together with some feldspar[2]

Table 1 – Description of the clay gouge materials used during the current study. [1] Highley, (1984): [2] Donohew *et al.* (2000).

	Experiment	Sample Material	Type of test	Slip-plane orientation	Reactivation pore press (MPa)	Vertical stress (MPa)					Shear stress (MPa)				
						Average	Start	Yield	Peak	Reactivation	Start	Shear modulus	Yield	Peak	Reactivation
1	ASR_BigCCS_07K	Kaolinite	Fault reactivation with water	30°	2.17	2.67	2.44	2.50	2.66	2.70	0.75	316	1.37	1.58	1.51
2	ASR_BigCCS_08K	Kaolinite			2.17	2.59	2.44	2.50	2.67	2.69	0.72	318	1.39	1.71	1.53
3	ASR_BigCCS_09K	Kaolinite			1.95	2.62	2.45	2.51	2.68	2.65	0.74	302	1.37	1.62	1.47
4	ASR_BigCCS_10K	Kaolinite			3.34	5.13	4.77	4.84	5.14	5.16	1.21	386	2.44	3.21	3.07
5	ASR_BigCCS_11K	Kaolinite			2.45	3.88	3.57	3.67	3.90	3.92	0.98	396	2.08	2.41	2.39
6	ASR_BigCCS_12K	Kaolinite			3.31	6.35	5.92	5.99	6.38	6.41	1.53	431	3.09	4.12	3.91
7	ASR_BigCCS_13K	Kaolinite			2.56	3.86	3.62	3.70	3.88	3.89	0.98	359	1.97	2.32	2.29
8	ASR_BigCCS_14BC	Ball Clay			1.27	2.65	2.46	2.47	2.67	2.66	0.92	236	1.27	1.51	1.50
9	ASR_BigCCS_15BC	Ball Clay			1.17	3.85	3.62	3.75	3.91	3.89	1.13	293	2.06	2.28	2.26
10	ASR_BigCCS_16BC	Ball Clay			1.74	5.06	4.82	4.88	5.07	5.07	1.65	403	2.33	2.98	2.96
11	ASR_BigCCS_17BC	Ball Clay			2.80	6.27	6.00	6.08	6.30	6.30	2.01	436	2.99	3.60	3.57
12	ASR_BigCCS_18BC	Ball Clay			1.19	5.04	4.83	4.88	5.08	5.08	1.71	401	2.38	2.89	2.88
13	ASR_BigCCS_19BC	Ball Clay			2.75	6.20	6.04	6.08	6.27	6.25	2.38	149	2.62	2.96	2.95
14	ASR_BigCCS_20K	Kaolinite	#1	30°	/	5.34	5.92	6.01	6.26	/	1.53	453	3.19	3.94	/
15	ASR_BigCCS_21K	Kaolinite	#2		/	6.17	5.93	6.04	6.31	/	1.51	489	3.46	3.96	/
16	ASR_BigCCS_22Kg	Kaolinite	Fault reactivation with gas	30°	/	4.99	4.72	4.84	5.10	/	1.33	399	2.36	3.07	/
17	ASR_BigCCS_23Kg	Kaolinite			1.65	2.57	2.41	2.45	2.61	2.60	0.65	318	1.33	1.58	1.56
18	ASR_BigCCS_24Kg	Kaolinite			/	3.76	3.60	3.67	3.78	/	0.96	386	1.93	2.36	/
19	ASR_BigCCS_25Kg	Kaolinite			/	6.21	5.92	6.05	6.29	/	1.04	905	3.26	3.98	/
20	ASR_BigCCS_26Kg	Kaolinite			/	2.58	2.38	2.46	2.62	/	0.64	316	1.28	1.58	/
21	ASR_BigCCS_27Kg	Kaolinite			/	1.13	1.00	1.07	1.15	/	0.44	149	0.59	0.68	/
22	ASR_BigCCS_28Kg	Kaolinite			/	3.82	3.57	3.66	3.89	/	1.32	283	1.77	2.22	/
23	ASR_BigCCS_29Ksh	Kaolinite	Stress history tests	30°	/	6.16	5.96	6.08	6.27	/	1.61	333	3.30	3.89	/
24	ASR_BigCCS_30Ksh	Kaolinite			/	6.19	5.96	6.06	6.31	/	1.53	445	3.32	3.88	/
25	ASR_BigCCS_31Ksh	Kaolinite			/	6.17	5.95	6.07	6.29	/	1.58	431	3.21	3.87	/
26	ASR_BigCCS_32Ksh	Kaolinite			/	6.19	5.95	6.07	6.27	/	1.56	428	3.21	3.93	/
27	ASR_BigCCS_33Ksh	Kaolinite			/	3.55	3.55	3.55	3.54	/	0.78	436	0.78	0.78	/
28	ASR_BigCCS_34Ksh	Kaolinite			/	6.21	5.93	6.06	6.30	/	1.57	445	3.14	3.91	/

Table 2 – List of all experiments undertaken as part of the current study. #1 = stress history test, mechanical data only reported here; #2 = flow test, only mechanical test reported here.

Relationship	Starting shear stress			Yield shear stress			Peak shear stress			Reactivation pressure		
	Slope	Intercept	R^2	Slope	Intercept	R^2	Slope	Intercept	R^2	Slope	Intercept	R^2
Kaolinite[1]	0.30	/	0.84	0.61	/	0.99	0.72	/	0.99	0.63	/	0.39
Kaolinite[2]	0.25	0.24	0.88	0.61	0.00	0.99	0.74	-0.11	0.99	0.37	1.14	0.91
Ball Clay[1]	0.41	/	0.93	0.55	/	0.90	0.63	/	0.88	0.36	/	0.56
Ball Clay[2]	0.44	-0.13	0.93	0.46	0.45	0.93	0.56	0.38	0.90	0.38	-0.09	0.56

Table 3 – Relationship between vertical and shear stress for kaolinite and Ball Clay gouge. Note condition (1) has the intercept set as 0, whereas condition (2) does not.

Parameter		Kaolinite[1]	Kaolinite[2]	Ball Clay[1]	Ball Clay[2]	Average[1]	Average[2]
Coefficient of friction	μ	0.717	0.738	0.634	0.561	0.697	0.706
Cohesion (MPa)	C	/	(-0.09)	/	0.33	/	(-0.4)
R^2		0.99	0.99	0.88	0.90	0.96	0.96
Angle of internal friction	ϕ	35.6	36.4	32.4	29.2	34.9	35.2
Fault angle	θ	27.2	26.8	28.8	30.4	27.6	27.4

Table 4 – Shear properties of the test gouge. Note condition (1) has the intercept set as 0, whereas condition (2) does not. Linear regression has resulted in two tests showing a negative cohesion, these are shown in parenthesis as cohesion should not be less than zero for these experiments.

Test	Gas entry pressure (MPa)	Maximum gas pressure (MPa)	Reactivation pressure (MPa)
ASR_BigCCS_22Kg	/	5.35	
ASR_BigCCS_23Kg	2.40	5.58	4.71
ASR_BigCCS_24Kg	2.26	5.58	
ASR_BigCCS_25Kg	2.27	5.66	
ASR_BigCCS_26Kg	2.29	5.57	
ASR_BigCCS_27Kg	2.19	5.80	
ASR_BigCCS_28Kg	2.39	5.54	
Average	2.30	5.58	4.71

Table 5 – Gas testing properties.